processes

MDPI

Article

Reservoir Characteristics of Tight Sandstone in Different Sedimentary Microfacies: A Case Study of the Triassic Chang 8 Member in Longdong Area, Ordos Basin

Jianchao Shi [1], Likun Cao [1], Baishun Shi [1], Shuting Shi [1], Xinjiu Rao [1], Xinju Liu [1], Wangyikun Fan [2], Sisi Chen [2] and Hongyan Yu [2,*]

[1] Exploration and Development Research Institute of Petro China Changqing Oilfield Company, Xi'an 710018, China; jianchao1851@163.com (J.S.); likuncao1258@126.com (L.C.); baishunshi175@126.com (B.S.); shutingshi158@126.com (S.S.); xinjiurao258@163.com (X.R.); x1371105@163.com (X.L.)

[2] State Key Laboratory of Continental Dynamics, Department of Geology, Northwest University, Xi'an 710069, China; fanwangyikun@163.com (W.F.); sisichen19988@163.com (S.C.)

* Correspondence: author: yuhy@nwu.edu.cn

Abstract

The complexity of tight sandstone reservoirs challenges effective oil and gas exploration. The Chang 8 Member of the Yanchang Formation in the Longdong area of the Ordos Basin has significant exploration potential. However, its reservoir characteristics are controlled by two distinct provenance systems and diverse sedimentary microfacies. The specific impacts of these factors on reservoir quality and their relative importance have remained unclear. This study employs an integrated analytical approach combining casting thin sections, conventional porosity-permeability measurements, and Nuclear Magnetic Resonance (NMR) to systematically investigate the petrological characteristics, pore structure, and physical properties of the Chang 8 reservoirs. Our findings reveal that the entire section of Chang 8 is a delta front subfacies, with sub sections of Chang 8^1 and 8^2 developing microfacies such as underwater distributary channels, underwater natural levees, sheet sand and mouth bars. The tight sandstone reservoir is mainly composed of lithic arkose and feldspathic litharenite, with its porosity dominated by dissolution and intergranular types. These secondary pores, particularly those resulting from feldspar dissolution, are of great importance. The underwater distributary channels have the best pores, followed by sheet sands, and underwater natural levees the worst. Compaction in Chang 8^2 is stronger than in Chang 8^1, leading to smaller pores. The northwest provenance is characterized by high clay content and small pores, while the southwest provenance has coarser grain size and better-preserved intergranular pores. Reservoir properties improve toward the lake but deteriorate at the lake-proximal end due to more small pores. This study reveals the control laws of sedimentary microfacies, provenance, and diagenesis on the pore development of tight sandstone in the Longdong area, providing theoretical guidance for the exploration and development of tight sandstone oil and gas in the region.

Keywords: pore structure; sedimentary microfacies; tight sandstone reservoir; provenance system; Chang 8 sub-member; Ordos Basin

check for updates

Academic Editor: Qiang Yu

Received: 16 September 2025
Revised: 9 October 2025
Accepted: 11 October 2025
Published: 12 October 2025

Citation: Shi, J.; Cao, L.; Shi, B.; Shi, S.; Rao, X.; Liu, X.; Fan, W.; Chen, S.; Yu, H. Reservoir Characteristics of Tight Sandstone in Different Sedimentary Microfacies: A Case Study of the Triassic Chang 8 Member in Longdong Area, Ordos Basin. *Processes* **2025**, *13*, 3246. https://doi.org/10.3390/pr13103246

Copyright: © 2025 by the authors. Licensee MDPI, Basel, Switzerland. This article is an open access article distributed under the terms and conditions of the Creative Commons Attribution (CC BY) license (https://creativecommons.org/licenses/by/4.0/).

1. Introduction

Tight sandstones are extensively developed in major petroliferous basins worldwide, including those in North America, the Middle East, and China, and have become increas-

ingly critical as unconventional reservoirs for oil and gas exploration [1–3]. In contrast to conventional reservoirs, tight sandstones are characterized by very low porosity, ultra-low permeability, and complex pore-throat systems, which collectively hinder fluid flow and hydrocarbon recovery [4–6]. With growing global energy demand and the continuous depletion of conventional resources, tight sandstones have gained prominence as a strategic alternative for future exploration and development. However, their strong heterogeneity—driven by the interplay of sedimentary microfacies, provenance supply, and diagenetic history—makes reservoir quality prediction exceptionally challenging [7–9]. Thus, investigating the origin and evolution of pore systems in these rocks is essential not only for understanding reservoir genesis but also for formulating effective exploration and production strategies in such unconventional systems.

In China, tight sandstones are widely distributed in several large sedimentary basins, such as the Ordos, Sichuan, and Songliao basins, and have become key targets for unconventional resource development [10–12]. Significant progress has been made in recent decades in unraveling their sedimentary architecture, diagenetic evolution, and hydrocarbon accumulation mechanisms [13,14]. However, most previous studies have focused on macroscopic sedimentological features or isolated diagenetic processes [10,15,16]. For example, some works are limited to a single provenance system, failing to compare pore evolution pathways under different sediment supplies. Others have not sufficiently addressed the pronounced differences in compaction intensity and porosity between the Chang 8^1 and Chang 8^2 sub-members. More importantly, a comprehensive framework integrating the synergistic effects of sedimentary microfacies, provenance, and diagenesis on pore development is still lacking. This knowledge gap limits the accurate prediction of reservoir quality and constrains the efficient development of tight sandstone resources in China.

The Ordos Basin is one of the most important hydrocarbon-bearing basins in China, where the Triassic Yanchang Formation hosts substantial accumulations in tight sandstone reservoirs. In the Longdong area, the Chang 8 Member is influenced by two distinct provenance systems and a range of delta-front microfacies, which collectively govern reservoir heterogeneity. Although previous research has advanced our understanding of the Yanchang Formation's sedimentology, diagenesis, and hydrocarbon accumulation [17,18], the specific controls of microfacies, provenance, and diagenesis on pore characteristics remain poorly quantified. This is particularly evident for the Chang 8^1 and Chang 8^2 sub-members, which exhibit clear differences in compaction intensity, pore types, and microfacies assemblages—yet the mechanisms underlying these variations are still not fully understood.

To address these issues, this study focuses on the tight sandstones of the Triassic Yanchang Chang 8 Member in the Longdong area of the Ordos Basin. Using an integrated methodology that incorporates casting thin sections, conventional porosity-permeability measurements, and nuclear magnetic resonance (NMR) analysis, we systematically investigate the petrological characteristics, pore types, and pore-throat structure of reservoirs formed under different sedimentary microfacies and provenance conditions. Furthermore, we clarify how sedimentary microfacies, provenance supply, and diagenetic processes collectively govern pore evolution. The results offer a theoretical foundation for the effective exploration and development of tight sandstone oil and gas in this region.

2. Geological Setting

Ordos Basin is a large polycyclic cratonic basin encompassing multiple tectonic and sedimentary systems. With an area of approximately 37×10^4 km^2, it is rich in oil, natural gas, coal, and other mineral resources [19,20]. The basin can be divided into six primary

tectonic units: the Yimeng Uplift, West Margin Thrust Belt, Tianhuan Depression, Yishan Slope, Weibei Uplift, and Jinxi Flexure Belt [21,22]. Internally, the basin exhibits a relatively simple tectonic framework, characterized by stable sedimentation, limited faulting, and gently dipping strata that are nearly horizontal, with dip angles generally less than 1° [23]. It forms an asymmetric syncline with a broad and gentle eastern limb and a narrow, steep western limb. The northern and southern ends of the syncline dip inward, giving the basin a roughly rectangular shape elongated in a north-south direction [24].

The basin has undergone multiple episodes of tectonic activity of varying scales and intensities, including both extensional and compressional events. These include the Precambrian Fuping, Wutai, and Lüliang movements, as well as the later Caledonian, Indosinian, Yanshanian, and Himalayan tectonic phases, which collectively shaped its present geomorphic framework [25]. During the Late Triassic, the Indosinian movement caused widespread regional uplift, resulting in higher topography in the north and lower relief in the south. Influenced by multi-phase strike-slip compression and marginal thrust-nappe from the Qinling-Qilian fold orogenic belt, the basin experienced continuous subsidence, evolving into a foreland-style flexural basin with a steep southwestern margin and a gentle northeastern slope [25]. The Late Triassic represented a complete developmental cycle of an inland freshwater lake basin, during which the Upper Triassic Yanchang Formation was deposited, exceeding 1000 m in thickness. This formation constitutes the principal oil-bearing sequence in the region [26]. Composed mainly of terrigenous clastic rocks, the Yanchang Formation records fluvial, deltaic, and lacustrine depositional environments and is widely distributed across the basin [27,28].

Yanchang Formation represents an inland lake-delta sedimentary system [29,30] and is subdivided into ten members, designated Chang 1 through Chang 10 from top to bottom [31,32]. Lake expansion initiated during the Chang 10 to Chang 8 depositional periods, reaching its maximum extent in the Chang 7 stage. From Chang 6 to Chang 1, the lake basin gradually shrank and eventually disappeared [33]. The Chang 8 Member was deposited between the initial lake flooding surface and the maximum flooding surface. Due to rapid subsidence and uplift cycles, deltaic systems advanced and retreated frequently over short periods, leading to the accumulation of large-scale, vertically stacked, and laterally continuous tight sandstones [34]. The Chang 8 Member can be further divided into two sub-members, Chang 8^1 and Chang 8^2, based on sedimentary cycles. Both sub-members have relatively stable thicknesses, generally ranging from 35 to 45 m.

The study area is situated in the southwestern part of the Yishan Slope tectonic unit, adjacent to the Tianhuan Depression to the west (Figure 1). It features a gentle north-south-trending monocline with simple structural development. Only a few small-scale nose-like structures are present, whereas large-scale fractures, folds, and faults are uncommon. The region covers about 50,000 km^2 and contains several oilfields with reserves on the order of 100 million tons. Among these, the tight sandstone reservoirs of the Chang 8 Member, formed during the peak phase of lake basin development, contain the most concentrated oil accumulations in the area. During Chang 8 deposition, the study area was located in a delta-front subfacies where underwater distributary channel sand bodies formed the most favorable hydrocarbon reservoirs [32].

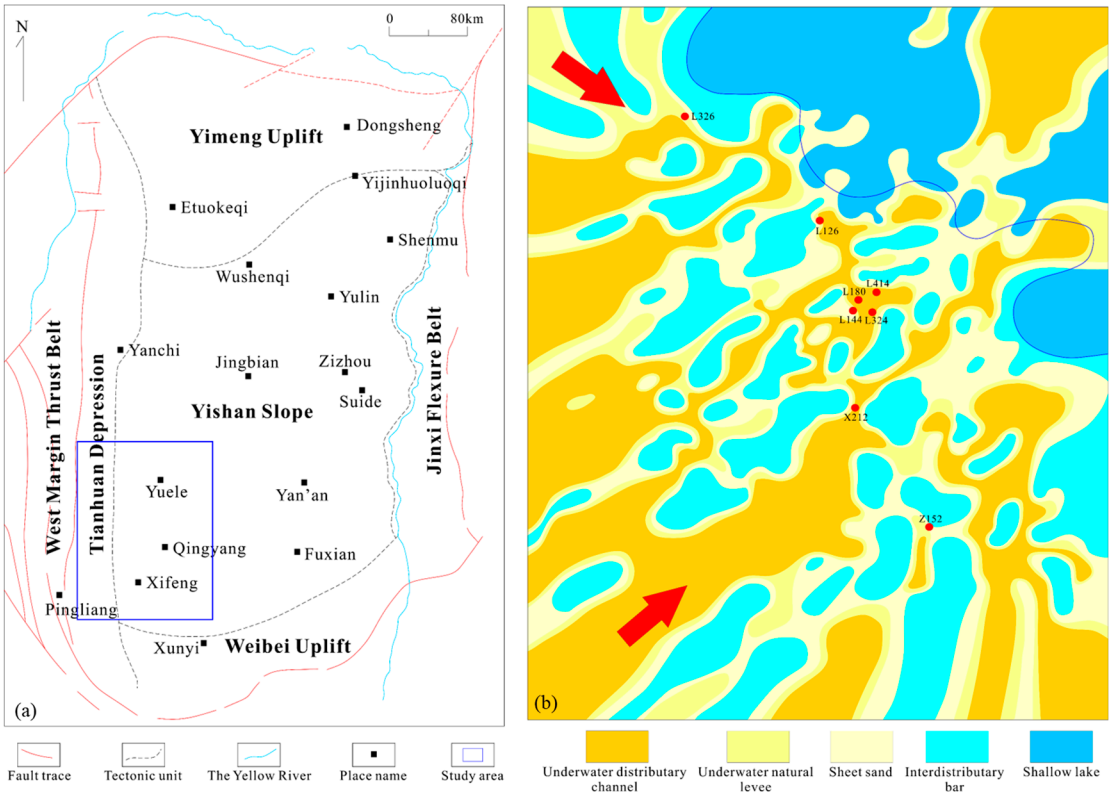


Figure 1. (**a**) Tectonic divisions of the Ordos Basin showing the location of the study area; (**b**) Sedimentary microfacies distribution and sampling points of the Chang 8 Member in the Longdong area, the red dots represent coring experimental Wells.

3. Materials and Methodology

3.1. Sampling and Petrophysical Properties

Core samples were collected from 17 wells penetrating the Chang 8 Member in the Longdong area, primarily targeting the main oil-producing intervals, the Chang 8^1 and Chang 8^2 sub-members. A systematic sampling approach was adopted to support porosity and permeability analysis.

Prior to analysis, residual hydrocarbons and salts were removed from the samples through solvent extraction, followed by oven-drying at 100 °C for 24 h. Porosity was measured using a CM300 overburden porosity-permeability analyzer. Permeability was determined based on Darcy's law through repeated measurements under varying pressure conditions. For mineralogical analysis, the samples were ground to a powder with a particle size of less than 10 μm and evenly packed into sample grooves. After instrument calibration and diffraction data acquisition, phase composition and crystal structure were identified using software-assisted spectrum analysis, based on the diffraction behavior of X-rays interacting with crystalline materials.

3.2. Nuclear Magnetic Resonance (NMR) Experiment

Nuclear Magnetic Resonance (NMR) is a widely used technique for characterizing fluids in subsurface reservoirs by exploiting the magnetic resonance properties of hydrogen nuclei (^{1}H) in a static magnetic field. The principle involves applying a stable magnetic field to align the hydrogen nuclei in formation water, generating a net macroscopic magnetic moment. A subsequent radiofrequency (RF) pulse of specific frequency excites these nuclei, causing them to absorb energy and transition to higher energy states, thereby altering their alignment. After the RF pulse ceases, the nuclei return to their equilibrium state through a process known as relaxation, releasing energy in the form of detectable signals. Key

relaxation parameters—longitudinal relaxation time (T1) and transverse relaxation time (T_2)—are measured during this process and are used to estimate reservoir properties such as porosity, fluid type, and permeability.

In this study, NMR measurements were conducted on six tight sandstone samples collected from underwater distributary channel microfacies under different provenance systems within the study area. Prior to testing, all samples were vacuum-dried at 105 °C for 48 h to remove residual moisture. Porosity was measured using the helium displacement method to minimize the influence of initial water content on sample swelling. All experiments were performed under constant temperature conditions (25 °C), and each measurement was completed within 30 min to limit ambient humidity effects.

The NMR instrument was operated according to the following procedure: the system was powered on, the magnet temperature was set, and the cooling unit was activated, followed by a preheating period exceeding 16 h. The pulse sequence was then selected to calibrate the scanning space and set relevant parameters. The saturated core sample was placed in a carbon fiber holder and positioned at the center of the measurement chamber. Finally, the appropriate pulse sequence and parameters were applied to initiate measurements at scheduled intervals. A T_2 cutoff value of 33 ms was employed to effectively characterize the pore structure of the tight sandstone samples.

3.3. Petrological and Mineralogical Analysis

To characterize the petrology and mineral composition of the tight sandstone samples, casting thin sections and X-ray diffraction (XRD) analyses were performed.

A total of 29 representative core plugs from different microfacies and well locations were selected for casting thin section preparation. The samples were first vacuum-impregnated with blue epoxy resin to highlight pore spaces. They were then cut, polished to a standard thickness of 30 μm, and covered with glass slides. The thin sections were examined using a Leica DM2700P polarizing microscope to identify mineral compositions, grain contacts, pore types (e.g., intergranular, intragranular dissolved), and diagenetic features (e.g., cementation, compaction). Photomicrographs were captured under both plane-polarized and cross-polarized light.

Whole-rock XRD analysis was conducted to quantitatively determine the mineralogical composition. After removing any carbonate cement with dilute hydrochloric acid, the samples were crushed and ground to a fine powder (<10 μm). The powdered samples were then packed into sample holders and analyzed using a Panalytical X'Pert Pro diffractometer with Cu-Kα radiation, operating at 40 kV and 40 mA. Data were collected over a 2θ range of 3° to 65° with a step size of 0.02°. The mineral identification and semi-quantitative weight percentages were determined using the X'Pert HighScore Plus software (version 2.1) and reference intensity ratio (RIR) methods.

4. Results and Discussion

4.1. Depositional Facies

During the deposition of the Chang 8 Member, sediment supply was relatively stable, mainly from the southwest with a minor contribution from the northwest. Transport along gentle slopes near the source areas led to the development of a shallow-water braided river delta system, dominated by medium- to fine-grained distributary channel sandstones formed under strong traction currents. The Ordos Basin inherited the large-scale transgressive pattern from the underlying Chang 9 period, resulting in shore–shallow lacustrine deposits in the Chang 8^2 sub-member. As the southwestern provenance advanced, delta-front subfacies became widespread. By the time of Chang 8^1 deposition, transgression had ceased, the base level dropped rapidly, and the southwestern source continued to prograde,

leading to an expanded deltaic scale and greater progradation distance. This caused the lake shoreline to migrate consistently landward (Figure 2).

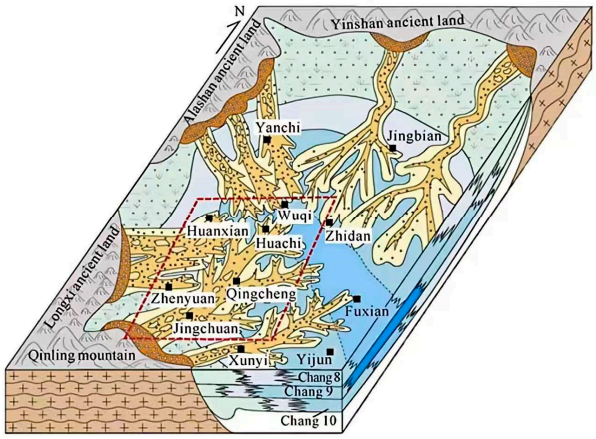


Figure 2. Sketch map of the deposition patterns of the Chang 8 members in the Ordos Basin [35].

Four principal microfacies are recognized within the Chang 8 Member sandbodies: underwater distributary channels, underwater natural levees, mouth bars, and sheet sands (Table 1). The characteristics of each microfacies are summarized as follows.

Table 1. Quantitative identification criteria for principal microfacies in the Chang 8 Member.

Microfacies	Lithology	GR Shape	GR (API)	Typical Thickness (m)
Underwater Distributary Channel	Medium- to fine-grained sandstone	Box-shaped	65–90	5–12
Underwater Natural Levee	Interbedded sandstone, siltstone and mudstone	Bell-shaped	85–110	2–5
Mouth Bar	Fine-grained sandstone and siltstone	Funnel-shaped	70–100	3–8
Sheet Sand	Argillaceous sand-stone/silty mudstone	Finger-like	95–130	1–4

1. Underwater distributary channels, composed of gray to dark-gray, medium- to fine-grained sandstones with massive bedding and frequent scour surfaces, which represent high-energy depositional conditions under strong traction currents. It exhibits a characteristic box-shaped gamma-ray (GR) log response (typically 65–90 API).
2. Underwater natural levees consist of interbedded gray sandstones, siltstones, and gray-black mudstones, deposited under lower-energy conditions. It shows a bell-shaped GR response (typically 85–110 API). These deposits are characterized by limited thickness and restricted lateral continuity.
3. Mouth bars composed mainly of fine-grained sandstones and siltstones, displaying a distinct coarsening-upward succession indicative of progradation and shallowing water depth. Typically reflected by a funnel-shaped GR log response (typically 70–100 API).

4. Sheet sands formed by alternating sandstones, siltstones, and mudstones under low-energy, stable conditions. Represented by finger-like (or serrated) GR log signatures (typically 95–130 API).

These diverse depositional environments produced pronounced heterogeneity in the lithofacies architecture and tight sandstone reservoir characteristics of the Chang 8 Member.

4.2. Petrological Characteristics

The reservoir is predominantly composed of lithic arkose and feldspanthic litharenite, followed by arkose and litharenite based on the sandstone thin-section observations and X-ray diffraction (XRD) experimental data from a total of 59 samples across the study area. The compositional distribution of each microfacies, as detailed in Figure 3, is supported by a robust dataset (e.g., n = 26) for underwater distributary channels), ensuring its regional representativeness. The average mineral composition consists of approximately 40.55% quartz, 33.55% feldspar, and 25.9% rock fragments. Consistent with this overall composition, sandstones from the underwater distributary channel, underwater natural levee, sheet sand, and mouth bar microfacies are also dominated by lithic arkose and arkosic litharenite. Arkose is additionally present in the underwater distributary channel facies (Figure 3).

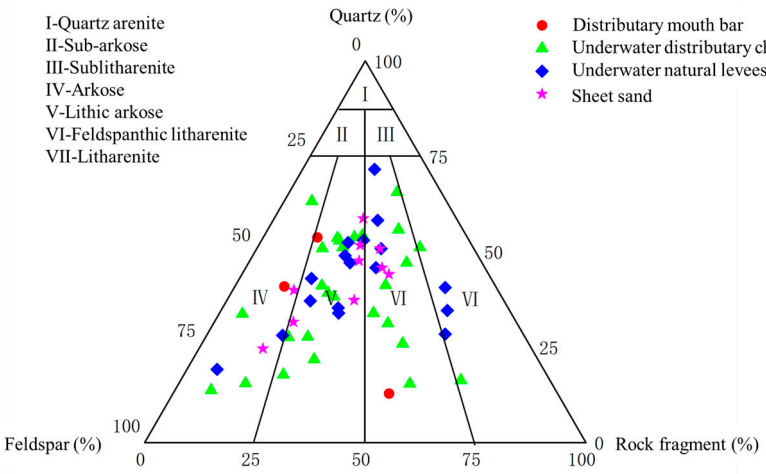


Figure 3. Ternary diagram illustrating the framework compositions of Chang 8 derived from X-ray diffraction analysis in the study area. The number of samples (n) for each microfacies is as follows: underwater distributary channels (n = 26), underwater natural levees (n = 15), sheet sands (n = 15), and mouth bars (n = 3).

Mineral compositions vary distinctly among the different microfacies. Underwater natural levees and sheet sands exhibit quartz contents exceeding 40% (42.83% and 43.87%, respectively). This quartz enrichment enhances compaction resistance, aiding the preservation of primary pores [15,36]. In contrast, mouth bars are characterized by higher feldspar (40.03%) and carbonate mineral (11.67%) contents. Although these minerals are prone to dissolution and can generate secondary porosity, they also promote cementation, which may impair reservoir quality [37,38]. Underwater distributary channels contain the highest clay mineral content (18.12%), which significantly influences pore structure by occupying pore space and reducing permeability (Figure 4).

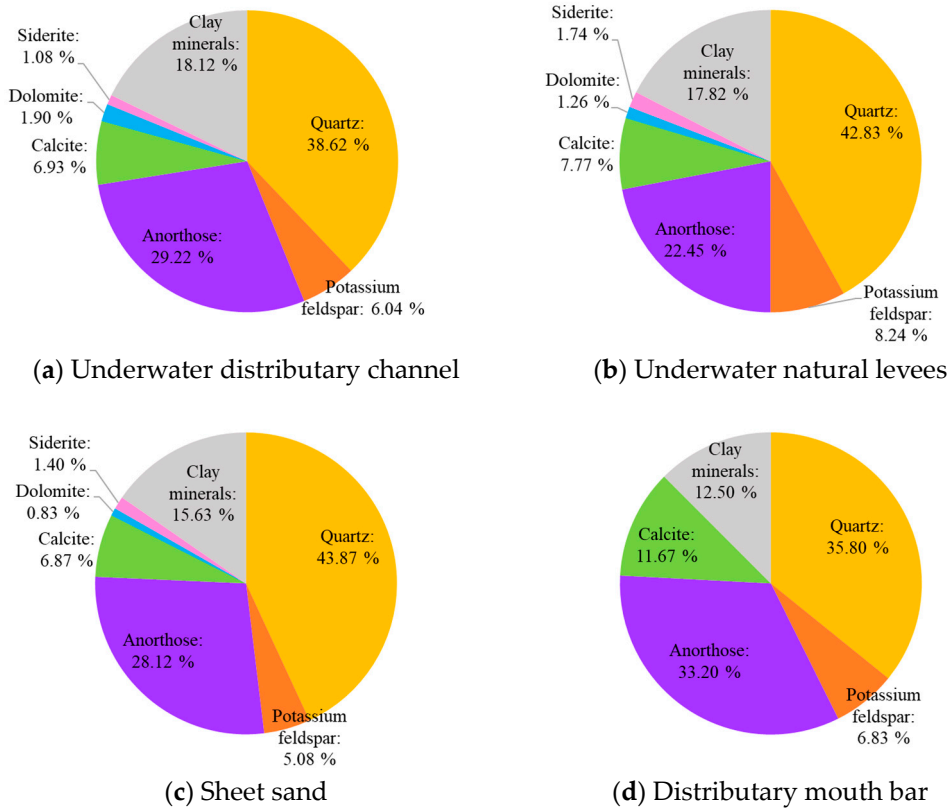


Figure 4. Mineral composition of tight sandstones from different sedimentary microfacies of the Chang 8 Member, as determined by X-ray diffraction (XRD) analysis. The pie charts compare the relative contents of quartz, feldspar, clay minerals, and carbonate minerals in (**a**) underwater distributary channel, (**b**) underwater natural levee, (**c**) sheet sand, and (**d**) distributary mouth bar deposits.

Overall, quartz, plagioclase, and clay minerals are the principal components across all microfacies, though their relative abundances vary considerably. These compositional differences are closely tied to hydrodynamic conditions and depositional settings. Stronger hydrodynamics in distributary channels promoted clay mineral transport and accumulation, whereas natural levees and sheet sands experienced greater winnowing, enriching more stable quartz grains. Mouth bars, formed under weaker hydrodynamic conditions, favored the deposition and preservation of feldspar and carbonate minerals. These mineralogical variations not only reflect depositional environments specific to each microfacies but also exert a primary control on diagenetic evolution and reservoir quality in the Chang 8 Member.

Significant variations in mineral composition and clay mineral assemblages are observed across different well blocks and depositional settings. In lake-distal well blocks, the contents of quartz, feldspar, and clay minerals remain relatively stable, with potassium feldspar being notably more abundant than in lake-proximal blocks. Well blocks located within channel centers show relatively higher quartz content, while calcite increases progressively from lake-distal to lake-proximal areas. The L326 well block, situated in the northwest provenance system near the lake margin, contains minor amounts of dolomite and calcite.

Clay mineral compositions also exhibit systematic spatial patterns. Illite–smectite (I/S) mixed-layer clays are nearly absent in lake-distal well blocks, where only trace amounts of kaolinite occur. Toward the lake center, I/S content first increases and then decreases, while kaolinite shows a steady increasing trend. Within the northwest provenance system,

the L326 well block is characterized by relatively low chlorite content compared to the southwest provenance system, but higher abundances of illite and kaolinite.

4.3. Physical Properties

The physical properties of the different microfacies exhibit pronounced contrasts. The underwater distributary channel facies exhibit the most favorable reservoir characteristics, with porosity predominantly ranging from 6% to 8% and permeability concentrated in the 0.01–0.05 mD range (Figure 5a), reflecting consistently good reservoir quality. The underwater natural levee facies rank second, showing porosity mainly between 4% and 8%, and permeability distributed across both the 0.01–0.05 mD and 0.1–0.5 mD intervals (Figure 5b). Although slightly inferior to the distributary channels, this microfacies still possesses moderate reservoir potential.

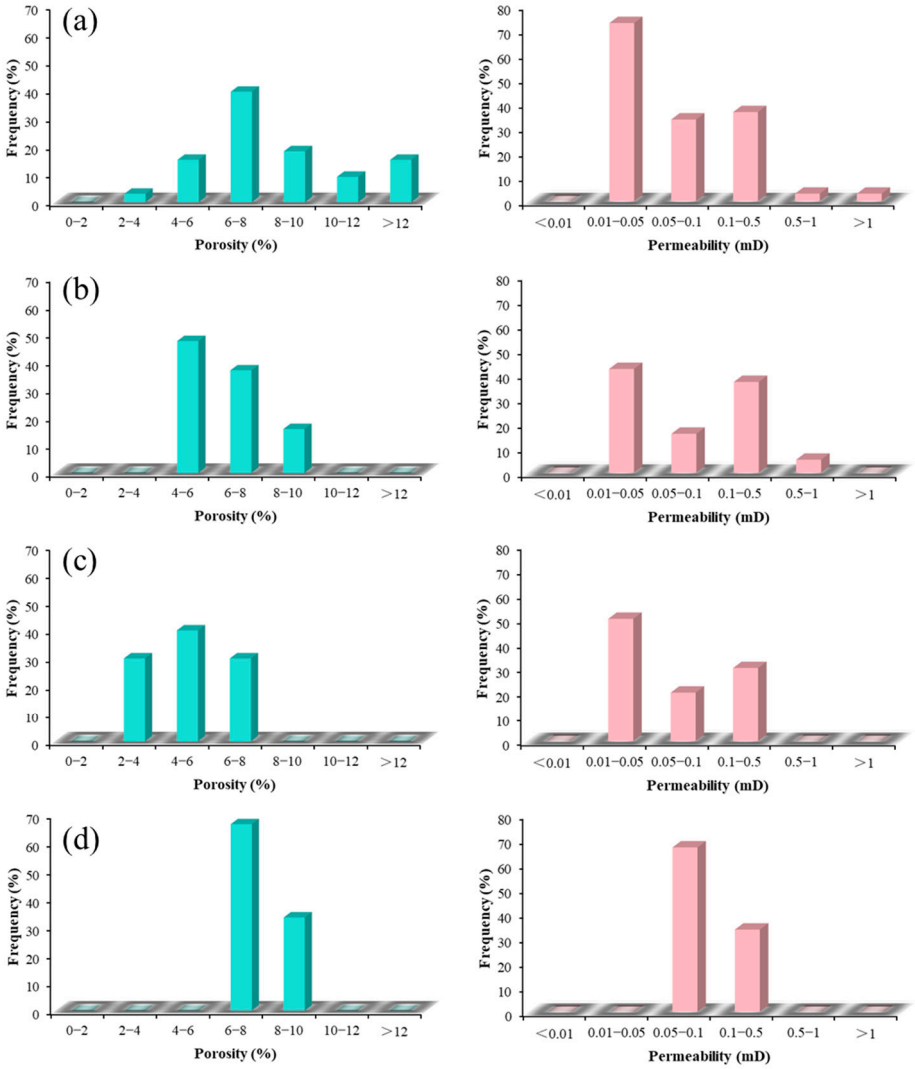


Figure 5. Comparison of petrophysical properties (porosity and permeability) of tight sandstones from different sedimentary microfacies of the Chang 8 Member, (**a**) Underwater distributary channel; (**b**) Underwater natural levees; (**c**) Sheet sand; (**d**) Distributary mouth bar.

In contrast, sheet sands are characterized by fine grain size, high shale content, and a predominance of argillaceous sandstone, resulting in poor reservoir performance. Porosity in this microfacies is mainly between 2% and 6%, with permeability concentrated in the low ranges of <0.01 mD and 0.01–0.05 mD (Figure 5c). Mouth bars, though only locally developed, show porosity values concentrated in the 6–8% range—with some samples

even higher—and permeability primarily in the 0.01–0.05 mD interval (Figure 5d). Where sufficiently developed, mouth bars can also constitute relatively high-quality reservoirs.

The porosity distribution across the study area generally follows a normal distribution, dominated by ultra-low (<5%) and extra-low (5–10%) values, with the peak interval concentrated between 5% and 10%. This indicates an overall limited pore space, classifying the reservoir as a low-porosity system. Porosity gradually improves toward the lake center, likely due to stronger wave or tidal reworking near the lake that reduced argillaceous matrix content and helped preserve primary pores. However, in well blocks closest to the lake margin, porosity shows a marked deterioration, characterized by an increase in micropores and a reduction in macropores. This decline is attributed to the prevalence of fine-grained, shale-rich sediments, such as sheet sands or shoreline muds—combined with enhanced cementation during diagenesis, which collectively infilled pore spaces.

Permeability follows a similar spatial trend, primarily falling within the ultra-low (<0.1 mD) and extra-low (0.1–1 mD) ranges, peaking between 0.01 mD and 0.5 mD, which reflects generally poor fluid flow capacity. Consistent with porosity, permeability increases lakeward, corresponding to coarser grain size and improved pore connectivity. By contrast, lake-proximal well blocks display the lowest permeability values across the study area, all within the ultra-low range. These patterns confirm that argillaceous infilling and diagenetic cementation significantly restrict pore-throat connectivity and impede fluid migration.

Overall, reservoir heterogeneity in the Chang 8 Member is governed by the interplay of sedimentary microfacies, provenance, hydrodynamic energy, and diagenesis. Stronger hydrodynamics promote quartz enrichment and primary pore preservation, while weaker energy or clay-rich deposition encourages pore occlusion through compaction and cementation. The combined influence of these factors controls the spatial variability in reservoir quality and the development of high-porosity, high-permeability sandbodies within the delta-front system.

4.4. Pore Structures Characterization Under Different Microfacies

The tight reservoirs of the Chang 8 Member contain four main pore types: intergranular pores, intragranular dissolved pores (mainly from feldspar dissolution), intergranular dissolved pores (resulting from cement dissolution), and microfractures. Of these, intergranular and feldspar-dissolved pores are the most abundant. Residual intergranular pores typically show regular shapes and straight grain contacts, indicating limited impact from diagenetic dissolution or cementation [39]. In contrast, dissolved pores form during diagenesis through the reaction of acidic fluids with soluble minerals such as feldspar, carbonate cements, or sulfate minerals, resulting in pores of variable size and irregular morphology [40]. Observations from cast thin sections confirm that feldspar is the dominant soluble mineral in these reservoirs.

Pore development shows clear spatial variations that correlate closely with hydrodynamic conditions and provenance. Although both Well X212 and Well L324 are located in underwater distributary channels within the southwest provenance system, they differ significantly along a lakeward gradient. Toward the lake, the abundance and size of intergranular and feldspar-dissolved pores decrease (Figure 6a–d), indicating diminished hydrodynamic energy. Well X212, situated closer to the sediment source, experienced stronger currents that helped preserve primary intergranular pores and promoted feldspar dissolution, enhancing secondary porosity. In contrast, Well L324, located nearer to the lake, contains more argillaceous matrix, which infills primary pores and suppresses feldspar dissolution, leading to poorer pore development. Grain contacts transition from point-type at X212 to concave-convex at L324, accompanied by finer grain size, better sorting (subrounded grains), and a shift to matrix-supported fabric. Increased deformation of

plastic fragments at L324 further reflects stronger compaction and densification, collectively reducing pore space and confirming the lakeward decline in reservoir quality.

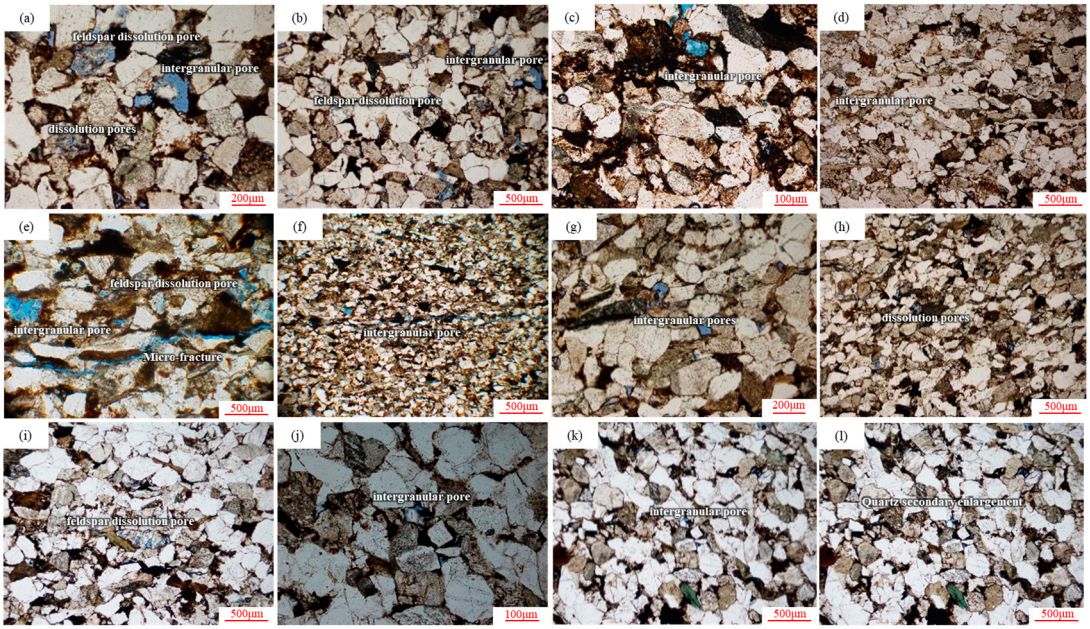


Figure 6. Thin section images for pore structure characteristics in sandstone samples: (**a**) intergranular pore, intragranular dissolution pores formed by the dissolution of feldspar, Well X212, 2202.47 m, Chang 8^1 sub-member, underwater distributary channel; (**b**) intergranular pore, intragranular dissolution pores, Well X212, 2202.5 m, Chang 8^1 sub-member, underwater distributary channel; (**c**,**d**) intergranular pores, Well L324, 1978.34 m, Chang 8^1 sub-member, underwater distributary channel; (**e**) intergranular pores, Well L326, 2637.96 m, Chang 8^1 sub-member, underwater natural levee; (**f**) intergranular pores, feldspar dissolution pores and micro-fracture, Well L326, 2617.7 m, Chang 8^1 sub-member, underwater natural levee; (**g**) intergranular pores, Well B20, 1905.64 m, Chang 8^1 sub-member, underwater natural levee; (**h**) dissolution pores, Well B20, 1905.64 m, Chang 8^1 sub-member, underwater natural levee; (**i**) intragranular dissolution pores formed by the dissolution of feldspar, Well L126, 2160.76 m, Chang 8^1 sub-member, sheet sand; (**j**,**k**) intergranular pores, Well L126, 2160.76 m, Chang 8^1 sub-member, sheet sand; (**l**) quartz secondary enlargement, Well L126, 2160.76 m, Chang 8^1 sub-member, sheet sand.

Provenance-controlled differences are also evident in the underwater natural levee microfacies. Despite belonging to the same microfacies, Wells L326 (northwest provenance) and B20 (southwest provenance) exhibit markedly different reservoir characteristics. L326 displays smaller grain size, better sorting, predominantly line and concave-convex grain contacts, abundant plastic components, and reservoir spaces dominated by intergranular pores, feldspar dissolution pores, and microfractures (Figure 6e,f). Intense compaction has resulted in highly densified reservoirs. In contrast, B20 exhibits coarser grains, poorer sorting, fewer plastic components, and better preservation of both primary and secondary pores (Figure 6g,h). These contrasts reflect systematic variations in sedimentary energy, transport distance, and diagenetic intensity controlled by provenance.

The sheet sand microfacies, as exemplified by Well L126, is characterized by fine-grained, well-sorted sediments with a high proportion of plastic components and concave–convex grain contacts. Strong compaction has limited the development of both intergranular and dissolved pores (Figure 6i–l), resulting in very poor reservoir quality.

The tight sandstone reservoirs of the Chang 8 Member exhibit significant heterogeneity, governed by the combined effects of sedimentary microfacies, provenance, hydrodynamic conditions, and diagenesis. Reservoir quality is generally highest in underwater distribu-

tary channels, moderate in natural levees and mouth bars, and poorest in sheet sands, reflecting contrasts in grain size, sorting, clay content, and pore structure development. Intergranular and feldspar-dissolved pores are the dominant pore types. Higher hydrodynamic energy promotes the preservation of primary pores and the formation of secondary porosity, whereas lower energy conditions and clay-rich, fine-grained deposition enhance compaction and cementation, reducing pore space. Reservoir quality generally improves toward the lake center due to coarser grains and enhanced pore connectivity but deteriorates near the lake margin where fine-grained sediments and diagenetic filling dominate. The distribution of clay minerals further reflects provenance input and diagenetic history, collectively controlling the spatial distribution of high-quality reservoirs within the delta-front system.

The Chang 8^2 sub-member shows better development of primary pores compared to the Chang 8^1 sub-member, a feature closely related to the presence of chlorite coatings. These coatings help resist compaction, preserve primary pores, and reduce pore-space loss during diagenesis [41]. Significant spatial variations are also observed along the lakeward direction within underwater distributary channels. Reservoirs closer to the lake center display fewer intergranular and feldspar-dissolved pores, with many pores filled by clay minerals (Figure 7a–d). This is likely due to weakened hydrodynamics near the lake, which reduces clay transport capacity and promotes depositional infilling. Grain contacts transition from line to concave-convex types, indicating stronger compaction. In addition, mica minerals show pronounced bending and deformation, further confirming intense compaction and increased reservoir densification. These trends reflect the combined influence of declining hydrodynamic energy and enhanced diagenetic intensity on reservoir properties along the lakeward gradient.

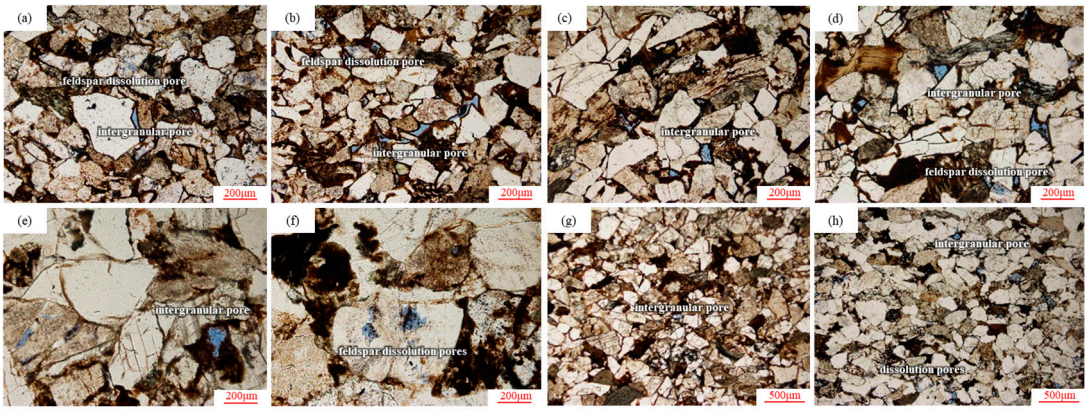


Figure 7. Thin section images for pore structure characteristics in sandstone samples: (**a**,**b**) intergranular pore and intragranular dissolution pores formed by the dissolution of feldspar, Well Z152, 1871.26 m, Chang 8^2 sub-member, underwater distributary channel; (**c**) intergranular pores, Well L144, 2292.82 m, Chang 8^2 sub-member, underwater distributary channel; (**d**) intergranular pores and feldspar dissolution pores, Well L144, 2292.82 m, Chang 8^2 sub-member, underwater distributary channel; (**e**) intergranular pores, Well Z152, 1871.26 m, Chang 8^2 sub-member, underwater natural levee; (**f**) feldspar dissolution pores, Well Z152, 1871.26 m, Chang 8^2 sub-member, underwater natural levee; (**g**) intergranular pores and dissolution pores, Well L414, 2300.04 m, Chang 8^2 sub-member, mouth bar; (**h**) intergranular pores and dissolution pores, Well L414, 2300.04 m, Chang 8^2 sub-member, mouth bar.

In the Chang 8^2 sub-member, the underwater natural levee microfacies is characterized by poorly sorted but relatively coarse grains, reflecting fluctuating hydrodynamic conditions during deposition. Strong currents transported coarse-grained material, while abrupt energy reductions led to rapid deposition of fine sediments, resulting in mixed grain sizes.

This microfacies experienced stronger compaction compared to the Chang 8^1 sub-member, as evidenced by predominantly concave–convex contacts, subordinate line contacts, and significant compression of primary pores. Mica minerals show pronounced bending and folding, and intergranular spaces are filled with quartz overgrowths and carbonate cements, which considerably reduce permeability. The reservoir is largely matrix-supported, with argillaceous material infilling intergranular gaps and further restricting pore connectivity. Well Z152, representative of this microfacies, is dominated by small pores with limited development of intergranular and feldspar-dissolved pores, resulting in poor reservoir performance (Figure 7e,f).

Sheet sands were deposited under weak and stable hydrodynamic conditions, resulting in fine-grained, poorly sorted sediments. Intense compaction has led to predominantly concave-convex grain contacts and a matrix-supported fabric, resulting in limited development of small intergranular pores and generally poor reservoir quality (Figure 7g). Mouth bar sandbodies exhibit similar concave-convex contacts, along with pronounced mica deformation, quartz overgrowths, and mica-filled fractures from crushed rigid grains, all indicating strong compaction. Characterized by matrix-supported texture, poor sorting, small pore size, and high heterogeneity, these sandbodies show restricted pore connectivity and overall low reservoir performance (Figure 7h).

The tight sandstones of the Chang 8^1 sub-member are composed of relatively coarse but poorly sorted grains, indicating deposition in an environment with ample sediment supply but unstable hydrodynamic conditions. The pore system is diverse, dominated by intergranular and feldspar-dissolution pores, along with minor intergranular dissolved pores and microfractures. Chlorite coatings on quartz grains help resist compaction, thereby preserving primary pores. As a result, the Chang 8^1 sub-member has undergone only moderate compaction, and its pore network remains relatively well preserved.

In contrast, the Chang 8^2 sub-member displays finer, poorly sorted grains and less developed porosity, dominated by intergranular pores with subordinate feldspar dissolution pores, resulting in more restricted reservoir space. Under compaction, rigid grains were fractured and subsequently infilled by mica, while widespread bending and deformation of mica further attest to strong compressional effects. These characteristics are particularly pronounced in the underwater natural levee and sheet sand microfacies of the Chang 8^2 sub-member, where intense compaction has considerably reduced pore volume, collectively leading to poorer reservoir physical properties compared to the Chang 8^1 sub-member.

Wells within the same underwater distributary channel microfacies but from different provenance systems also exhibit notable differences in reservoir characteristics. Well L324 shows a bimodal pore-size distribution, indicating a complex pore system with significant size variability. Its high quartz content and low calcite abundance minimize cement-related pore occlusion. Thin-section analysis reveals well-preserved intergranular pores, minor mica deformation, and intragranular dissolved pores, with intergranular clay occurring in reticular forms that do not severely limit connectivity. These attributes contribute to good porosity, permeability, and fluid mobility, resulting in superior reservoir quality.

Well L180 exhibits a unimodal to weakly bimodal T_2 distribution (Figure 8), reflecting a relatively uniform pore system dominated by small pores. Well-developed calcite cement has partially filled pore space. Although thin sections show clear quartz grain boundaries and both primary and secondary pores, overall compaction has reduced pore volume. The prevalence of small pores and homogeneous pore structure results in moderate reservoir quality, which is inferior to that of Well L324.

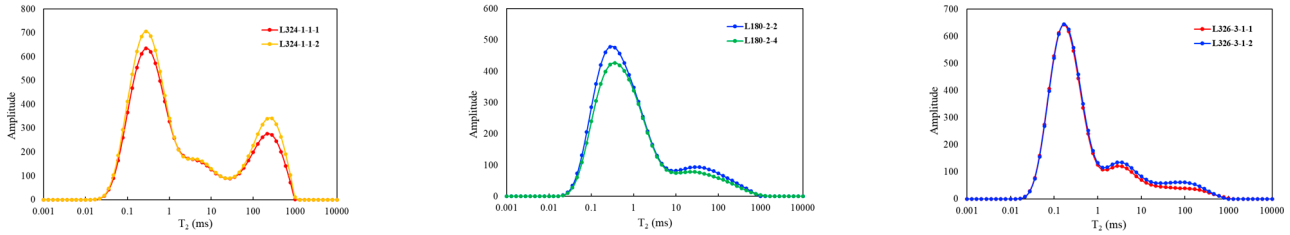


Figure 8. Comparison of T_2 spectra from three tight sandstone samples (L324, L180 and L326) collected from the underwater distributary channel of the Chang 8 Member.

Well L326, influenced by the northwest provenance, displays a bimodal to weakly trimodal T_2 distribution (Figure 8), indicating strong heterogeneity and a dominance of small pores. High feldspar content, combined with fine pore structure and intense compaction, has resulted in a dense reservoir with limited pore space. The sharp, short-T_2 peaks suggest a high proportion of micropores and restricted free fluid mobility. These distinctions stem from differences in sediment supply and transport dynamics between the northwestern and southwestern provenance systems. The northwest provenance tends to produce finer-grained sediments prone to developing smaller pores, and stronger compaction has further enhanced reservoir densification. As a result, the pore structure and fluid storage capacity of underwater distributary channel reservoirs vary considerably between these two provenance systems.

The tight sandstone reservoirs of the Chang 8 Member exhibit strong heterogeneity, with reservoir quality governed by the integrated effects of sedimentary microfacies, provenance, hydrodynamic conditions, and diagenesis. Underwater distributary channels generally possess the most favorable reservoir properties, characterized by well-preserved intergranular and feldspar-dissolution pores, moderate to high porosity, and good permeability. Natural levees and mouth bars show intermediate reservoir quality, whereas sheet sands display fine grain size, high clay content, strong compaction, and poorly developed porosity. Chlorite coatings and quartz-rich compositions help preserve primary pores and resist compaction, while fine-grained, clay-rich facies and extensive cementation reduce pore space and connectivity, particularly in proximal lake-margin settings. Spatially, reservoir properties improve significantly toward the lake (over ~80–100 km from the southwestern provenance) but deteriorate at the lake-proximal end (within the terminal 10–15 km) (e.g., from Well X212) toward the basin center, due to coarser grains, better sorting, and enhanced pore connectivity. However, this trend reverses within the terminal 10–15 km of the lake margin, defined as the “lake-proximal” zone where sandstone mud content exceeds 20% and porosity typically falls below 5%. In this zone, reservoir quality deteriorates markedly due to the dominance of fine-grained, shale-rich sediments (e.g., sheet sands) and intense diagenetic cementation.

Provenance also plays a key role in controlling reservoir heterogeneity. Sandstones derived from the southwestern provenance generally exhibit coarser grains, greater preservation of primary and secondary pores, and higher permeability, reflecting stronger hydrodynamic energy and moderate compaction. In contrast, those from the northwestern provenance tend to be finer-grained, richer in feldspar, and subject to stronger compaction, leading to a predominance of small pores, lower porosity, limited pore connectivity, and reduced fluid mobility. In summary, the interplay of microfacies, provenance, hydrodynamics, and diagenetic history collectively governs the spatial distribution of high-quality reservoirs and the development of pore systems, offering a coherent model for understanding the architecture and heterogeneity of delta-front tight sandstones in lacustrine basins.

The underwater distributary channel microfacies, particularly those influenced by the southwestern provenance, constitute the highest-quality “sweet spots” due to their coarser

grains, well-developed intergranular and dissolution pores, and superior connectivity. Therefore, exploration efforts should prioritize targeting these specific sedimentary units. Furthermore, the finding that reservoir quality generally improves in the lakeward direction (until the lake-proximal end where it deteriorates) provides a valuable spatial guideline for predicting the lateral extent of high-quality reservoirs and optimizing well trajectory design, especially for horizontal wells aimed at maximizing contact with the best reservoir facies.

Intervals dominated by sheet sands or areas with strong calcite cementation (as seen in some mouth bars) will exhibit higher fracture initiation pressures and may lead to complex, restricted fracture networks. Conversely, the more brittle, quartz-rich intervals of underwater distributary channels are more conducive to generating effective fracture networks. Pre-drill identification of these facies using seismic attribute analysis and log signatures can allow for customized, stage-by-stage fracturing designs. For instance, within a single horizontal well, stages landing in high-quality channel sandstones could utilize different fluid and proppant schedules compared to stages penetrating heterogeneous or tightly cemented intervals, thereby optimizing overall stimulation efficiency and production.

The prevalence of micropores and poor connectivity in reservoirs derived from the northwest provenance and in underwater natural levees suggests that these zones may exhibit rapid production decline and low recoverable volumes. Recognizing these facies helps in setting realistic production expectations and in planning for enhanced oil recovery (EOR) techniques at an early stage. For example, the abundance of clay minerals (especially illite/smectite) in certain facies, as identified in our study, warrants careful consideration of fracturing fluid chemistry to prevent formation damage.

5. Conclusions

In summary, this study demonstrates that the reservoir characteristics of the Chang 8 Member tight sandstones are systematically governed by the interplay of sedimentary microfacies, provenance, and diagenesis. The reservoir quality exhibits a clear spatial pattern: while it generally improves toward the lacustrine center due to enhanced hydrodynamics and pore connectivity, it deteriorates near the lake margin where fine-grained sedimentation and diagenetic filling promote micropore dominance. The content of illite-smectite mixed-layer clay also follows a predictable trend, initially increasing and then decreasing in the lakeward direction.

Significant differences in reservoir properties are observed among microfacies. Underwater distributary channels represent the highest-quality reservoirs, with porosity of 4–12% and permeability of 0.01–1 mD, characterized by well-developed dissolution and intergranular pores. Underwater natural levees show moderate properties (porosity 4–10%, permeability 0.01–0.5 mD) with poorly connected small pores, whereas sheet sands exhibit the poorest quality (porosity 2–6%). Furthermore, the Chang 8^2 sub-member experienced stronger compaction than the Chang 8^1 sub-member—partly because chlorite coatings in Chang 8^1 help resist compaction and preserve primary pores, as evidenced by extensive mica filling and grain deformation, resulting in narrower pores and stronger reservoir densification.

Provenance and hydrodynamic conditions ultimately control reservoir heterogeneity. The southwestern provenance, characterized by higher energy, yields quartz-rich sandstones with preserved primary pores and enhanced dissolution porosity, forming complex pore systems and favorable reservoirs. In contrast, the northwestern provenance, with weaker hydrodynamics, produces finer-grained, feldspar-rich sandstones with higher clay content. These undergo intense compaction, leading to a predominance of micropores and the least developed pore systems. This study confirms that provenance-driven sedimentary differentiation fundamentally shapes the formation and evolution of pore systems in tight sandstone reservoirs.

Author Contributions: Data curation, J.S., S.C. and X.R.; formal analysis, J.S.; funding acquisition, L.C.; investigation, J.S., L.C., X.L., S.C., H.Y. and X.R.; methodology, J.S., L.C., X.L., W.F. and H.Y.; project administration, L.C.; supervision, L.C., B.S. and S.S.; validation, L.C., B.S., S.S. and W.F.; writing—original draft, J.S.; writing—review & editing, X.L., W.F., S.C. and H.Y. All authors have read and agreed to the published version of the manuscript.

Funding: This research did not receive any specific grant from funding agencies in the public, commercial, or not-for-profit sectors.

Data Availability Statement: The original contributions presented in this study are included in the article. Further inquiries can be directed to the corresponding author.

Conflicts of Interest: The authors declare that they have no known competing financial interests or personal relationships that could have appeared to influence the work reported in this paper.

References

1. Hu, C.; Lin, Z.; Li, X.; Quaye, J.; Fu, Z. Tight sandstone reservoirs in lacustrine environments: Review and perspectives. *Int. Geol. Rev.* **2025**, *67*, 2236–2263. [CrossRef]
2. Ghanizadeh, A.; Clakson, C.; Aquino, S.; Ardakani, O.; Sanei, H. Petrophysical and geomechanical characteristics of Canadian tight oil and liquid-rich gas reservoirs: I. Pore network and permeability characterization. *Fuel* **2015**, *153*, 664–681. [CrossRef]
3. Schmoker, J. Resource-assessment perspectives for unconventional gas systems. *AAPG Bull.* **2002**, *86*, 1993–1999. [CrossRef]
4. Zou, C.; Zhu, R.; Liu, K.; Su, L.; Bai, B.; Zhang, X.; Yuan, X.; Wang, J. Tight gas sandstone reservoirs in China: Characteristics and recognition criteria. *J. Petrol. Sci. Eng.* **2012**, *88–89*, 82–91. [CrossRef]
5. Lai, J.; Wang, G.; Ran, Y.; Zhou, Z. Predictive distribution of high-quality reservoirs of tight gas sandstones by linking diagenesis to depositional facies: Evidence from Xu-2 sandstones in the Penglai area of the central Sichuan basin, China. *J. Nat. Gas Sci. Eng.* **2015**, *23*, 97–111. [CrossRef]
6. Su, S.; Jiang, Z.; Shan, X.; Zhu, Y.; Wang, P.; Luo, X.; Li, Z.; Zhu, R.; Wang, X. The wettability of shale by NMR measurements and its controlling factors. *J. Petrol. Sci. Eng.* **2018**, *169*, 309–316. [CrossRef]
7. Hu, Y.; Ma, Y.; Guo, B.; Gao, Z.; He, W. Application of stratigraphic-sedimentological forward modeling of sedimentary processes to predict high-quality reservoirs within tight sandstone. *Mar. Petrol. Geol.* **2019**, *101*, 540–555. [CrossRef]
8. Qiao, J.; Zeng, J.; Jiang, S.; Wang, Y. Impacts of sedimentology and diagenesis on pore structure and reservoir quality in tight oil sandstone reservoirs: Implications for macroscopic and microscopic heterogeneities. *Mar. Petrol. Geol.* **2020**, *111*, 279–300. [CrossRef]
9. Liu, M.; Xiong, C. Diagenesis and reservoir quality of deep-lacustrine sandy-debris-flow tight sandstones in Upper Triassic Yanchang Formation, Ordos Basin, China: Implications for reservoir heterogeneity and hydrocarbon accumulation. *J. Petrol. Sci. Eng.* **2021**, *202*, 108548. [CrossRef]
10. Yang, G.; Huang, D.; Huang, P.; Yan, W.; Yang, T.; Dai, H.; Lin, J. Control factors of high and stable production of Jurassic Da'anzhai Member tight oil in central Sichuan Basin, SW China. *Petrol. Explor. Dev.* **2017**, *44*, 866–875. [CrossRef]
11. Song, P.; Shi, J.; Liu, X.; Zhou, Y.; Yang, W.; Li, S.; Zhou, S.; Yu, H. Comprehensive Evaluation Method of the Tight Oil Reservoir Quality in the Ordos Basin. *Geofluids* **2025**, *1*, 7745871. [CrossRef]
12. Li, P.; Jia, C.; Jin, Z.; Liu, Q.; Zheng, M.; Huang, Z. The characteristics of movable fluid in the Triassic lacustrine tight oil reservoir: A case study of the Chang 7 member of Xin'anbian Block, Ordos Basin, China. *Mar. Petrol. Geol.* **2019**, *102*, 126–137. [CrossRef]
13. Ming, D.; Chang, X.; Shang, F.; Zhang, P.; Xu, Y.; Qu, Y.; Gao, W.; Ge, T.; Zhao, H. Heterogeneity of Pore Structure in Braided River Delta Tight Sandstone Reservoirs: Implications for Tight Oil Enrichment in the Jurassic Badaowan Formation, Central Junggar Basin. *Nat. Resour. Res.* **2025**, *34*, 1743–1771. [CrossRef]
14. Yao, Z.; Chen, D.; Tang, X.; Wang, Y.; Jiang, Z.; Yang, L.; Gao, Z. Pore Structure Formation Mechanism of Lacustrine Fine-Grained Sedimentary System in Fengcheng Formation, Junggar Basin, China. *Energy Fuels* **2025**, *39*, 7235–7253. [CrossRef]
15. Peng, J.; Hu, Z.; Feng, D. Influence of quartz types on rock fabrics and bulk physical properties in organic-rich mudstone: A review. *Earth-Sci. Rev.* **2024**, *249*, 104670. [CrossRef]
16. Wang, Z.; Zeng, L.; Chen, H.; He, F.; Liu, X. Impacts of Hydrocarbon Charging on Tight Sandstone Reservoirs: Chang 8 Member of Yanchang Formation in the Jinghe Oilfield, Southern Ordos Basin. *Geol. J.* **2025**, 1–15. [CrossRef]
17. Duan, Y.; Liu, X.; Wang, X.; Li, J.; Li, S.; Guo, R.; Chen, J.; Ma, X.; Li, X.; Zhang, S.; et al. Thermochronological Constraints on the Synchronisation of Reservoir Densification and Hydrocarbon Emplacement in the Upper Triassic Chang 8 Tight Sandstone, Ordos Basin. *Geol. J.* **2025**, 1–36. [CrossRef]
18. Zhang, K.; Li, S.; Zhong, G.; Feng, P.; Chang, C.; Li, H. Characteristics of in-situ stress field of coalbed methane reservoir in the eastern margin of Ordos basin. *Int. J. Coal Geol.* **2025**, *301*, 104715. [CrossRef]

19. Liu, Q.; Jin, Z.; Liu, W.; Lu, L.; Meng, Q.; Tao, Y.; Han, P. Presence of carboxylate salts in marine carbonate strata of the Ordos Basin and their impact on hydrocarbon generation evaluation of low TOC, high maturity source rocks. *Sci. China Earth Sci.* **2013**, *56*, 2141–2149. [CrossRef]
20. Feng, Z.; Dong, D.; Tian, J.; Zhou, S.; Wu, W.; Xie, C. Geochemical characteristics of the Paleozoic natural gas in the Yichuan-Huanglong area, southeastern margin of the Ordos Basin: Based on late gas generation mechanisms. *Mar. Petrol. Geol.* **2021**, *124*, 104867. [CrossRef]
21. Li, S.; Yao, J.; Mou, W.; Luo, A.; Wang, Q.; Deng, X.; Chu, M.; Li, Y.; Yan, C. The dissolution characteristics of the Chang 8 tight reservoir and its quantitative influence on porosity in the Jiyuan area, Ordos Basin, China. *J. Nat. Gas Geo.* **2018**, *3*, 95–108. [CrossRef]
22. Ji, L.; Yan, K.; Meng, F.; Zhao, M. The oleaginous botryococcus from the triassic Yanchang formationin Ordos Basin, Northwestern China: Morphology and its paleo environmental significance. *J. Asian Earth Sci.* **2010**, *38*, 175–185. [CrossRef]
23. Shang, T.; Chu, M.; Zhang, X.; Wang, B.; Li, J.; Zhang, H.; Zhang, Z.; Liu, X. Quantitative analysis of pore evolution and its application in basin simulation: A case study of Chang 6 reservoir in Heshui area, Ordos Basin, NW China. *Energy Geosci.* **2025**, *6*, 100403. [CrossRef]
24. Zhang, Q.; Yang, C.; Gu, Y.; Tian, Y.; Liu, H.; Xiao, W.; Wang, Z.; Mi, Z. Microscopic pore-throat structure and fluid mobility of tight sandstone reservoirs in multi-provenance systems, Triassic Yanchang formation, Jiyuan area, Ordos Basin. *Energy Geosci.* **2025**, *6*, 100407. [CrossRef]
25. Wang, W.; Yue, D.; Zhao, J.; Li, W.; Wang, B.; Wu, S.; Li, S. Diagenetic alteration and its control on reservoir quality of tight sandstones in lacustrine deep-water gravity-flow deposits: A case study of the Yanchang Formation, southern Ordos Basin, China. *Mar. Petrol. Geol.* **2019**, *110*, 676–694. [CrossRef]
26. Li, P.; Shen, B.; Liu, Y.; Bi, H.; Liu, Z.; Bian, R.; Wang, P.; Li, P. The fractal characteristics of the pore throat structure of tight sandstone and its influence on oil content: A case study of the Chang 7 Member of the Ordos Basin, China. *Petrol. Sci.* **2025**, *22*, 2262–2273. [CrossRef]
27. Gao, J.; Jin, Z.; Liang, X. Lacustrine organic carbon sequestration driven by volcanism: A case study of the third submember of the Chang 7 Member of the Yanchang Formation in the Ordos Basin. *Petrol. Sci.* **2025**, *22*, 3497–3511. [CrossRef]
28. Hou, X.; Hou, M.; Feng, Q.; Xiao, Y.; Lei, Z.; Lai, L.; Li, S.; Tian, H. High-resolution sequence stratigraphic framework and target sand bodies correlation of tight oil reservoirs in the Upper Triassic Yanchang Formation, Ordos Basin. *Petrol. Sci.* **2025**, 1–15. [CrossRef]
29. Wu, X.; Luo, H.; Zhang, J.; Chen, Q.; Fang, X.; Wang, W.; Li, W.; Shi, Z.; Zhang, Y. Volcanism-driven marine eutrophication in the end-Ordovician: Evidence from radiolarians and trace elements of black shale in South China. *J. Asian Earth Sci.* **2023**, *253*, 105687. [CrossRef]
30. Lei, Y.; Luo, X.; Wang, X.; Zhang, L.; Jiang, C.; Yang, W.; Yu, Y.; Cheng, M.; Zhang, Y. Characteristics of silty laminae in Zhangjiatan Shale of southeastern Ordos Basin, China: Implications for shale gas formation. *AAPG Bull.* **2015**, *99*, 661–687. [CrossRef]
31. Duan, Y. Geochemical characteristics of crude oil in fluvial deposits from Maling oilfield of Ordos Basin, China. *Org. Geochem.* **2012**, *52*, 35–43. [CrossRef]
32. Xi, K.; Cao, Y.; Liu, K.; Wu, S.; Yuan, G.; Zhu, R.; Kashif, M.; Zhao, Y. Diagenesis of tight sandstone reservoirs in the Upper Triassic Yanchang Formation, southwestern Ordos Basin, China. *Mar. Petrol. Geol.* **2019**, *99*, 548–562. [CrossRef]
33. Chen, S.; Yu, H.; Lu, M.; Lebedev, M.; Li, X.; Yang, Z.; Cheng, W.; Yuan, Y.; Ding, S.; Johnson, L. A new approach to calculate gas saturation in shale reservoirs. *Energy Fuels* **2022**, *36*, 1904–1915. [CrossRef]
34. Wang, G.; Chang, X.; Yin, W.; Li, Y.; Song, T. Impact of diagenesis on reservoir quality and heterogeneity of the Upper Triassic Chang 8 tight oil sandstones in the Zhenjing area, Ordos Basin, China. *Mar. Petrol. Geol.* **2017**, *83*, 84–96. [CrossRef]
35. Liu, H.; Yang, Y.; Wang, F.; Deng, X.; Liu, Y.; Nan, J.; Wang, J.; Zhang, H. Micro pore and throat characteristics and origin of tight sandstone reservoirs: A case study of the Triassic Chang 6 and Chang 8 members in Longdong area, Ordos Basin, NW China. *Petrol. Explor. Dev.* **2018**, *45*, 239–250. [CrossRef]
36. Nie, H.; Liu, Q.; Li, P.; Li, P.; Ding, J.; Sun, C.; Zhai, C.; Zhao, J.; Jin, Z.; Dang, W. Quartz types, formation mechanism, and its effect on shale oil and gas enrichment: A review. *Earth-Sci. Rev.* **2025**, *261*, 105011. [CrossRef]
37. Acuna-Uribe, M.; Lowe, D.; Azmy, K. Carbonate cement genesis and links to siliciclastic environments of deposition: Hibernia Formation, Jeanne d'Arc basin, offshore Newfoundland. *Mar. Petrol. Geol.* **2025**, *177*, 107379. [CrossRef]
38. Luo, T.; Guo, X.; He, Z.; Tao, Z.; Yun, N.; Huang, Y.; Wang, F.; Zhao, J. Natural gas accumulation and modification in the Precambrian carbonate reservoirs of the southwestern Sichuan Basin, China: Insight from pore fluid overpressure reconstruction and simulation. *J. Asian Earth Sci.* **2025**, *280*, 106451. [CrossRef]
39. Wang, Y.; Liu, L.; Li, S.; Ji, H.; Xu, Z.; Luo, Z.; Xu, T.; Li, L. The forming mechanism and process of tight oil sand reservoirs: A case study of Chang 8 oil layers of the Upper Triassic Yanchang Formation in the western Jiyuan area of the Ordos Basin, China. *J. Petrol. Sci. Eng.* **2017**, *158*, 29–46. [CrossRef]

40. Li, M.; Guo, Y.; Li, Z.; Wang, H. The diagenetic controls of the reservoir heterogeneity in the tight sand gas reservoirs of the Zizhou Area in China's east Ordos Basin: Implications for reservoir quality predictions. *Mar. Petrol. Geol.* **2020**, *112*, 104088. [CrossRef]
41. Wang, S.; Shan, X.; Yang, Q.; Wang, P.; He, W.; Xiao, M.; Liu, C.; Ma, X. Tight gas accumulation in middle to deep successions of fault depression slopes: Northern slope of the Lishu Depression, Songliao Basin. *Mar. Petrol. Geol.* **2025**, *174*, 107302. [CrossRef]

Disclaimer/Publisher's Note: The statements, opinions and data contained in all publications are solely those of the individual author(s) and contributor(s) and not of MDPI and/or the editor(s). MDPI and/or the editor(s) disclaim responsibility for any injury to people or property resulting from any ideas, methods, instructions or products referred to in the content.